ABSORBING BOUNDARY CONDITIONS*

Robert Clayton and Björn Engquist

ABSTRACT

Boundary conditions are derived for numerical wave simulation problems that minimize artificial reflections over a wide range of incident angles. The boundary conditions are based on paraxial approximations of the scalar and elastic wave equations. They are relatively inexpensive and simple to apply.

---

*This is a preprint of a paper we intend to submit for publication. Consequently we have not referenced articles that appear in the SEP reports. The bulk of the material is taken from the following papers in SEP-10:

Absorbing boundary conditions for wave equations, p. 30.
One way elastic wave equations, p. 125.
Difference approximations of one way waves, p. 141.

ABSORBING BOUNDARY CONDITIONS

Robert Clayton and Björn Engquist

Introduction

One of the persistent problems in the numerical simulation of wave phenomena is the artificial reflections that are introduced by the edge of the computational grid. These reflections, which eventually propagate inward and mask the true solution, necessitate the use of a much greater number of mesh points than would otherwise be required. Hence, it is of interest to develop boundary conditions that make the perimeter of the grid "transparent" to outward-moving waves.

One solution to the problem that has been proposed [Lysmer and Kuhlemeyer, 1969] is the viscous damping of normal and shear stress components along the boundary. This method approximately attenuates the reflected compressional waves over a wide range of incident angles to the boundary, but it does not diminish reflected shear waves as completely. Another method that can be made to work perfectly for all incident angles has been proposed by Smith [1973]. With this approach, the simulation is done twice: once with Dirichlet boundary conditions, and once with Neumann boundary conditions. Since these two boundary conditions produce reflections that are opposite in sign, the sum of the two cases will cancel the reflections. The chief shortcoming of this method is that the entire set of computations has to be repeated twice for each of the absorbing sides that are present.

In this paper we present a set of absorbing boundary conditions that are based on paraxial approximations (PA) of the scalar and elastic wave equations. A discussion of a similar type of boundary condition based on pseudodifferential operators, for a general class of differential equations, can be found in Engquist and Majda [1977]. The chief feature of the PA that we will exploit is that the outward-moving wavefield can be separated from the inward-moving one. Along the boundary, then, the PA can be used to model

only the outward-moving energy and hence minimize the reflections. The boundary conditions which we present are computationally efficient in that they require about the same amount of work per mesh point to apply as does the full wave equation.

In the first part of this paper, some paraxial approximations to the scalar and elastic wave equations are presented. In the second part, the PA are used as absorbing boundary conditions and expressions for the effective reflection coefficients along the boundary are given. Some numerical examples are presented in the final section.

Paraxial Approximations of the Wave Equation

Paraxial approximations of the scalar wave equation have been extensively developed by Claerbout [1970], [1971], [1976], and in the first part of this section we present a brief review of that work.

The two-dimensional wave equation

$$P_{xx} + P_{zz} = v^{-2} P_{tt} , \tag{1}$$

is usually considered for modelling purposes to be initial valued in time. The stability of the equation for time extrapolation is ensured by the fact that in its dispersion relation

$$\omega = v(k_x^2 + k_z^2)^{1/2} , \tag{2}$$

the frequency ω, is a real function of the spatial wave numbers k_x and k_z.

If we now consider spatial extrapolation of (1) (say, in the z-direction), the appropriate form of the dispersion relation would be

$$k_z = \pm \frac{\omega}{v} [1 - (v^2 k_x^2/\omega^2)]^{1/2} . \tag{3}$$

Clearly there are stability problems when $|v k_x/\omega| > 1$ (evanescent waves), because k_z becomes imaginary. It is therefore necessary to modify the wave equation in such a way as to eliminate the evanescent components of the solution. A relatively simple way of accomplishing this is to restrict the range of solutions to those waves that are traveling within a cone of the z-axis (paraxial waves).

To form the paraxial approximation of (1), we expand the square-root operator of (3) as a rational approximation about small vk_x/ω. Three such approximations are:

$$\text{A1:} \quad vk_z/\omega = 1 + O(|vk_x/\omega|^2) , \tag{4}$$

$$\text{A2:} \quad vk_z/\omega = 1 - \frac{1}{2}(vk_x/\omega)^2 + O(|vk_x/\omega|^4) , \tag{5}$$

$$\text{A3:} \quad \frac{vk_z}{\omega} = \frac{1 - \frac{3}{4}(vk_x/\omega)^2}{1 - \frac{1}{4}(vk_x/\omega)^2} + O(|vk_x/\omega|^6) . \tag{6}$$

A general order expansion, which leads to stable differencing schemes can be found by the recursion relation for a Padé series approximation to a square root [Muir, personal communication].

$$A_j = 1 - \frac{(vk_x/\omega)^2}{1 + A_{j-1}} + O\left(\left|\frac{vk_x}{\omega}\right|^{2j}\right) . \tag{7}$$

The dispersion relations A1, A2, A3, and the dispersion relation of the full wave equation are shown in Fig. 1.

The error term in the expansions indicates that the approximations are valid for waves traveling within a cone of the z-axis. We also note that in order to do the expansions it was necessary to choose one of the signs on the radical of (3). This indicates that incoming and outgoing wave fields are separated by the paraxial approximation.

In their differential form, Eqs. (4-6) appear as

$$\text{A1:} \quad P_z + \frac{1}{v} P_t = 0 , \tag{8}$$

$$\text{A2:} \quad P_{zt} + \frac{1}{v} P_{tt} - \frac{v}{2} P_{xx} = 0 , \tag{9}$$

$$\text{A3:} \quad P_{ztt} - \frac{v^2}{4} P_{zxx} + \frac{1}{v} P_{ttt} - \frac{3}{4} v P_{txx} = 0 . \tag{10}$$

Paraxial approximations for the elastic wave equation analogous to those of the scalar wave equation can also be found. We cannot, however, perform

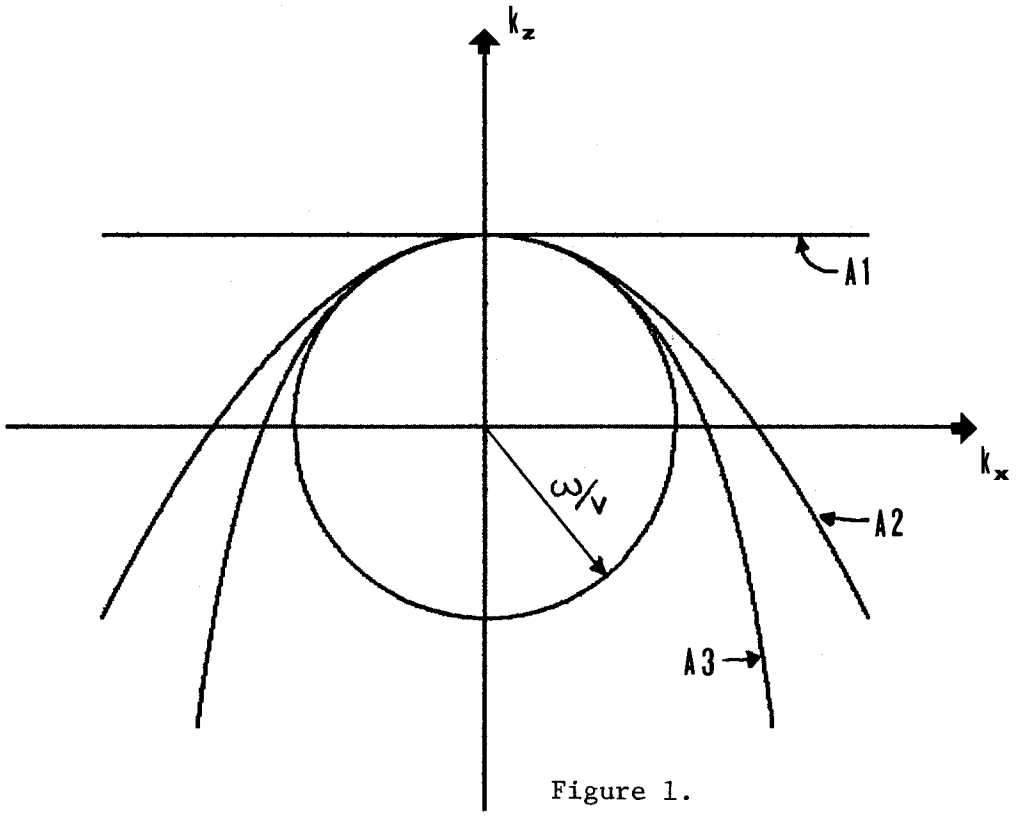

Figure 1.

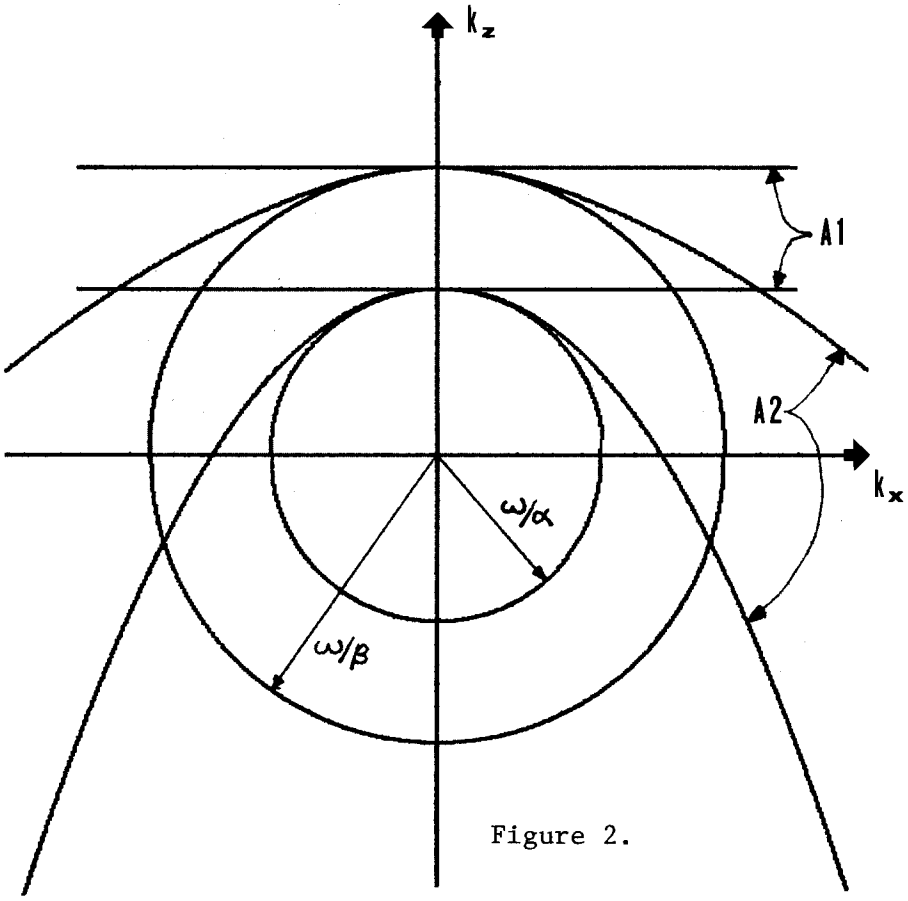

Figure 2.

the analysis by considering expansions of the dispersion relation because the differential equations for vector fields are not uniquely specified from their dispersion relations. Instead, we use the scalar case to provide a hint as to the general form of the paraxial approximation and fit the coefficients by matching to the full elastic wave equation.

We write the elastic wave equation for a homogeneous, isotropic medium in the form

$$\underline{u}_{tt} = D_1 \underline{u}_{xx} + H \underline{u}_{xz} + D_2 \underline{u}_{zz} \ , \tag{11}$$

where $$\underline{u} = \begin{pmatrix} u \\ w \end{pmatrix} = \begin{pmatrix} \text{horizontal displacement field} \\ \text{vertical displacement field} \end{pmatrix},$$

$$D_1 = \begin{pmatrix} \alpha^2 & 0 \\ 0 & \beta^2 \end{pmatrix}, \quad D_2 = \begin{pmatrix} \beta^2 & 0 \\ 0 & \alpha^2 \end{pmatrix}, \quad \text{and} \quad H = (\alpha^2 - \beta^2) \cdot \begin{pmatrix} 0 & 1 \\ 1 & 0 \end{pmatrix},$$

and α and β are the compressional and shear velocities, respectively. The Fourier Transform of this equation is

$$\left[I - D_1 \left(\frac{k_z}{\omega} \right)^2 - H \left(\frac{k_x}{\omega} \right) \left(\frac{k_z}{\omega} \right) - D_2 \left(\frac{k_x}{\omega} \right)^2 \right] \tilde{\underline{u}}(\ , k_x, k_z) = 0 \ . \tag{12}$$

We now consider two forms of the paraxial approximation

A1: $$\underline{u}_z + B_1 \underline{u}_t = 0 \ , \tag{13}$$

and

A2: $$\underline{u}_{tz} + C_1 \underline{u}_{tt} + C_2 \underline{u}_{tx} + C_3 \underline{u}_{xx} = 0. \tag{14}$$

The Fourier Transforms of these approximations are

A1: $$\left[I \left(\frac{k_z}{\omega} \right) - B_1 \right] \tilde{\underline{u}}(\omega, k_x, k_z) = 0 \ , \tag{15}$$

and

A2: $$\left[I \left(\frac{k_z}{\omega} \right) - C_1 + C_2 \left(\frac{k_x}{\omega} \right) - C_3 \left(\frac{k_x}{\omega} \right)^2 \right] \tilde{\underline{u}}(\omega, k_x, k_z) = 0. \tag{16}$$

In Eqs. (15) and (16), the (k_z/ω) term may be isolated and substituted in (12) to determine the coefficient matrices in (13) and (14). The results are:

$$B_1 = C_1 = \begin{pmatrix} 1/\beta & 0 \\ 0 & 1/\alpha \end{pmatrix},$$

$$C_2 = (\beta - \alpha)\begin{pmatrix} 0 & 1/\beta \\ 1/\alpha & 0 \end{pmatrix}, \qquad C_3 = \frac{1}{2}\begin{pmatrix} \beta - 2\alpha & 0 \\ 0 & \alpha - 2\beta \end{pmatrix}.$$

In Fig. 2 the dispersion relations for (17) and (18) are presented. The dispersion relations in this case are the loci of zeros of the determinant of the square-bracketed quantities in (15) and (16). The fact that there are two curves for each approximation indicates that they decouple into compressional and shear motions, as does the full wave equation. For the approximation A2, the shape of the dispersion curves depends on the ratio of α and β, and in Fig. 2 an α/β ratio of $\sqrt{3}$ is used. In general, the larger the velocity ratio becomes, the poorer the approximation for shear waves.

Absorbing Boundary Conditions

The dispersion curves presented in the previous section indicate that the paraxial approximations can be used to model waves moving in one general direction and to discriminate against waves moving in the opposite direction. To absorb incident energy along a given boundary then, we can use the paraxial approximation that models only energy moving outward from the interior of the grid toward that boundary. All of the approximations presented in the previous section modelled waves moving in the positive z-direction. Hence, on the grid shown in Fig. 3, they would be suitable for absorbing boundary conditions along the top edge. For the bottom edge, we would use the paraxial approximations which correspond to taking the negative sign on the radical of Eq. (3). In this case the dispersion relations would be approximating the lower half of the semi-circle. The boundary conditions for the sides are found by interchanging x and z in the two cases above.

To clarify the method we shall present the scheme used for the numerical examples in some detail. For each time step we:

(1) solved all interior points (cells labelled "i" in Fig. 3) with an explicit finite difference form of the full wave equation [Eqs. (1) or (11)]. See Kelly *et al.* [1976] for the difference formulae.

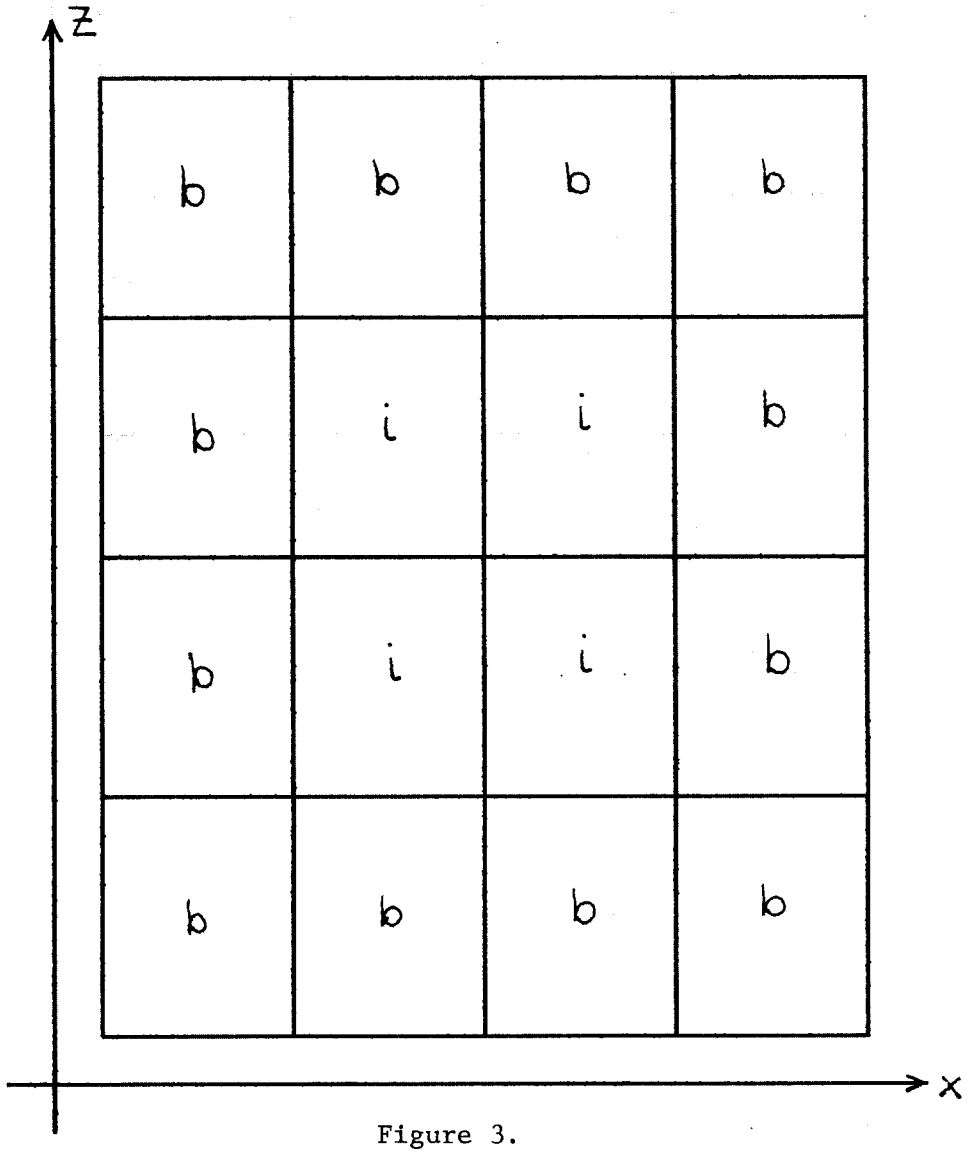

Figure 3.

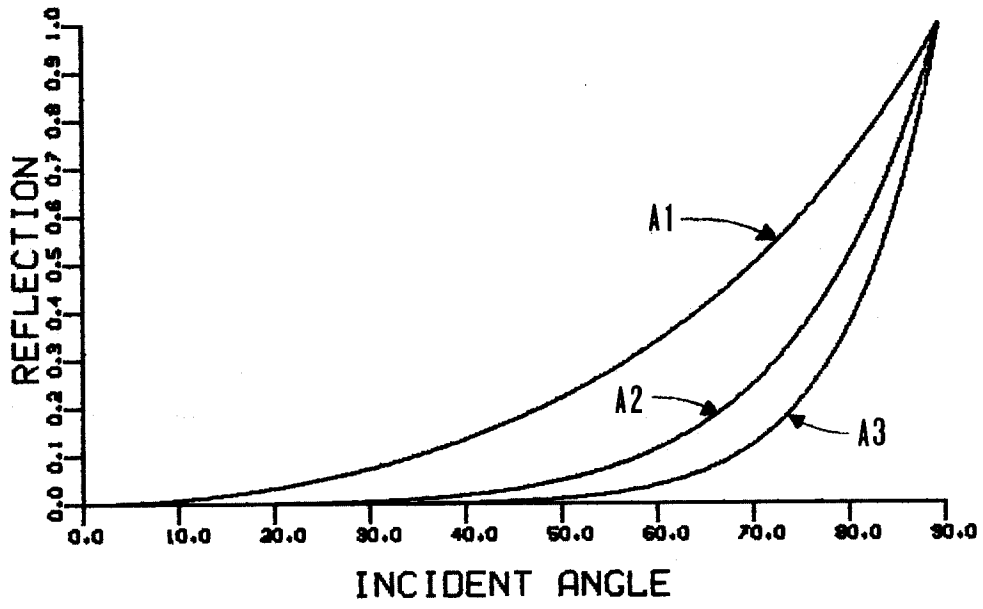

Figure 4.

(2) used the appropriate paraxial approximation to extrapolate spatially the interior solution one mesh row outward to fill in the boundary row (labelled "b" in Fig. 3). Since all of the paraxial approximations are first order in the spatial extrapolation direction, only the nearest interior row is needed for each boundary. The actual difference schemes are presented in the Appendix.

The effectiveness of the various absorbing boundary conditions given here can be gauged by comparing their effective reflection coefficients at the boundaries. For the scalar wave equation, consider an incident plane wave travelling in the positive z-direction,

$$P_I = \exp(i k_x x + i k_z z - i\omega t),$$

which initiates a reflection from the top boundary (at $z = 0$) of the form

$$P_R = c \exp(i k_x x - i k_z z - i\omega t) ,$$

where c is the effective reflection coefficient. Locally near the boundary, the wave field $P_I + P_R$ will satisfy both the boundary condition and the interior equation. Applying the boundary condition A2 for example, we obtain

$$k_z \omega (P_I - c P_R) - \left(\frac{\omega^2}{v} - \frac{v}{2} k_x^2 \right) (P_I + c P_R) = 0 .$$

Solving for c and evaluating at the boundary, we obtain

$$c = - \frac{1 - \frac{1}{2}(vk_x/\omega)^2 - (vk_z/\omega)}{1 - \frac{1}{2}(vk_x/\omega)^2 + (vk_z/\omega)} .$$

By noting that from the interior equation $(vk_x/\omega)^2 = 1 - (vk_z/\omega)^2$ and identifying vk_z/ω as $\cos\theta$ where θ is the angle of incidence measured from the normal to the boundary, we can write the reflection coefficient as

$$c(\theta) = - \left(\frac{1 - \cos\theta}{1 + \cos\theta} \right)^2 .$$

This expression may be generalized for the A_j boundary condition to

$$c_j(\theta) = - \left(\frac{1 - \cos\theta}{1 + \cos\theta} \right)^j .$$

In Fig. 4, the reflection coefficients for A1, A2, and A3 are plotted. It should be noted that angles where $c(\theta)$ is large correspond to waves travelling almost parallel to the boundary. They would therefore likely strike another absorbing boundary before interacting with the solution at the center of the grid. A measure of the energy radiated toward the center of the grid would be

$$[c_j(\theta)\ \sin\theta]^2.$$

To find the effective reflection coefficients for elastic waves, we assume plane wave potential solutions of the form

$$\Phi = P_I \exp i\ \frac{\omega}{\alpha}(\ell_\alpha x + n_\alpha z) + c_P \exp i\ \frac{\omega}{\alpha}(\ell_\alpha x - n_\alpha z)\ ,$$

$$\Psi = S_I \exp i\ \frac{\omega}{\beta}(\ell_\beta x + n_\beta z) + c_S \exp i\ \frac{\omega}{\beta}(\ell_\beta x - n_\beta z)\ ,$$

where ℓ_α, n_α, ℓ_β, and n_β are the direction cosines of the wave front. For incident compressional waves, $P_I = 1$ and $S_I = 0$, and for incident shear waves $P_I = 0$ and $S_I = 1$. The displacement fields are found by the transformation

$$u = \Phi_x + \Psi_z\ ,$$

$$w = \Phi_z - \Psi_x\ .$$

The expressions for the horizontal and vertical displacements are substituted into the time-transformed form of the boundary conditions A1 and A2, and the reflection coefficients c_P and c_S are determined. In Figs. 5 and 6, we show the reflection coefficients for the boundary conditions A1 and A2, respectively. The abrupt changes in reflection coefficients for incident shear waves are due to the formation of a pseudo-head wave along the boundary.

Numerical Examples

To illustrate the effectiveness of the boundary conditions, we present three examples. In each case, the computations were done with the usual Neumann (zero-slope) boundary conditions and with the A2 absorbing boundary conditions. A 40×40 grid was used with the mesh spacing chosen to make the explicit differencing scheme for the interior solution stable.

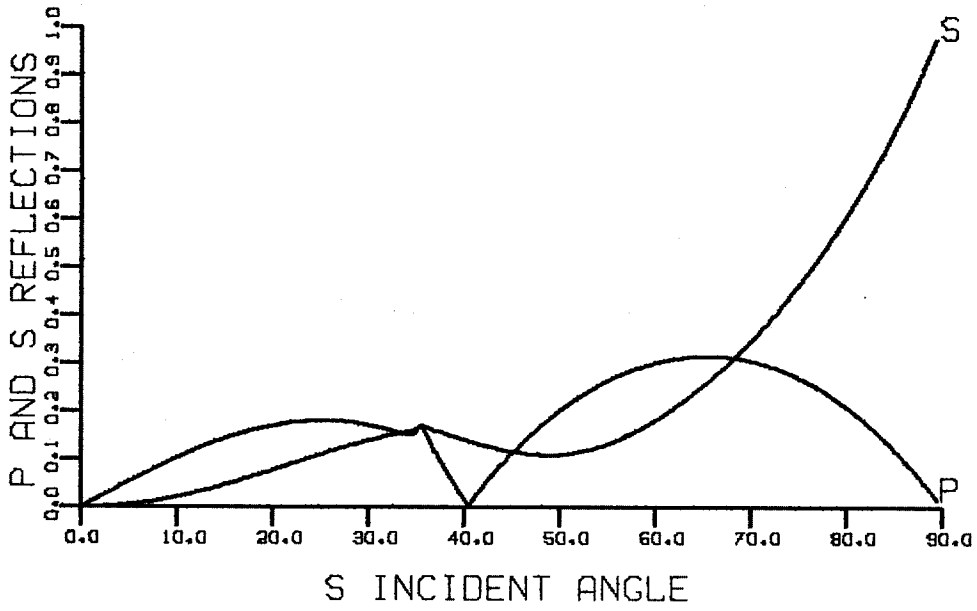
P AND S REFLECTIONS
0.0 0.1 0.2 0.3 0.4 0.5 0.6 0.7 0.8 0.9 1.0
S
P
0.0 10.0 20.0 30.0 40.0 50.0 60.0 70.0 80.0 90.0
S INCIDENT ANGLE

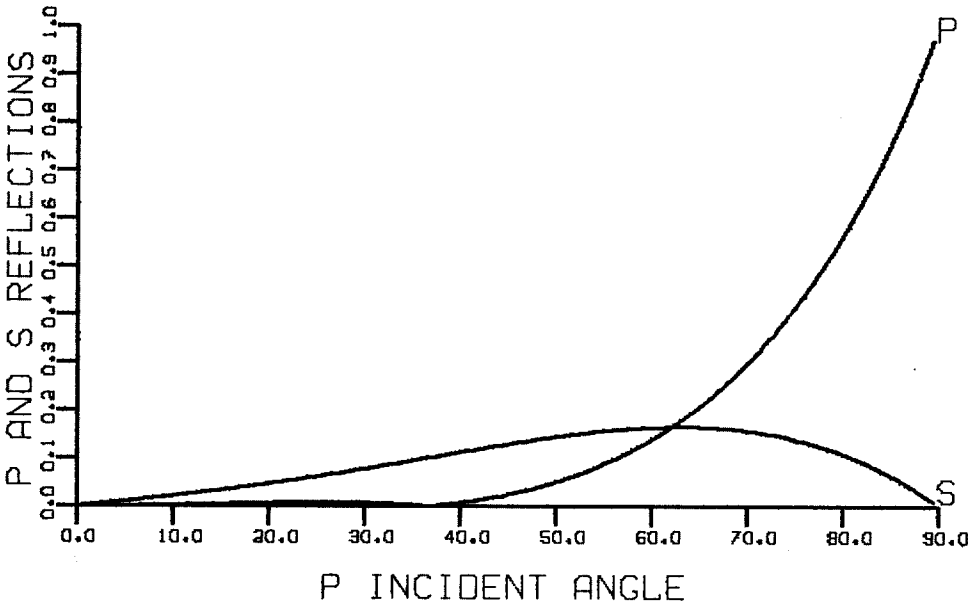
P AND S REFLECTIONS
0.0 0.1 0.2 0.3 0.4 0.5 0.6 0.7 0.8 0.9 1.0
P
S
0.0 10.0 20.0 30.0 40.0 50.0 60.0 70.0 80.0 90.0
P INCIDENT ANGLE

Figure 5.

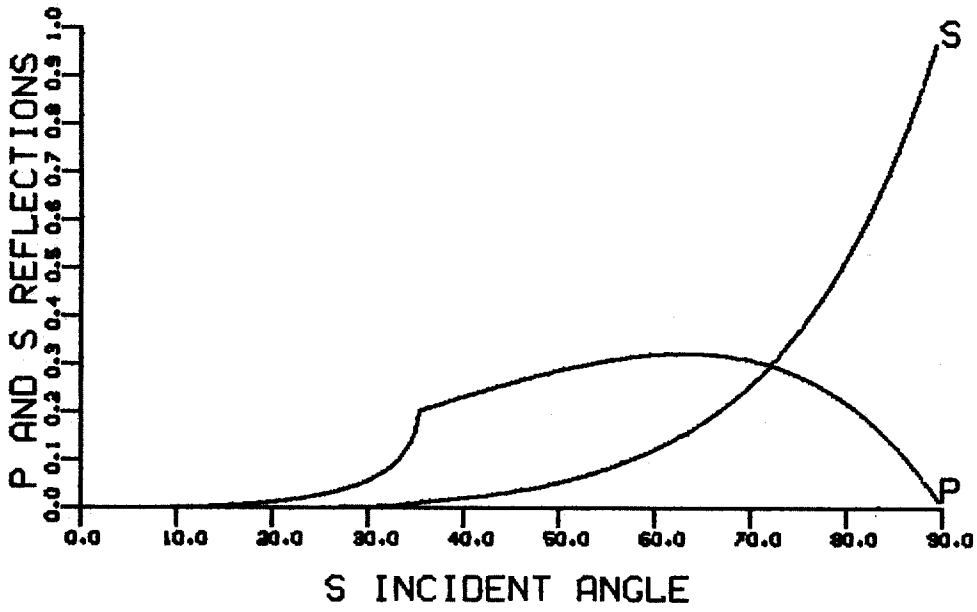
P AND S REFLECTIONS
0.0 0.1 0.2 0.3 0.4 0.5 0.6 0.7 0.8 0.9 1.0
S
P
0.0 10.0 20.0 30.0 40.0 50.0 60.0 70.0 80.0 90.0
S INCIDENT ANGLE

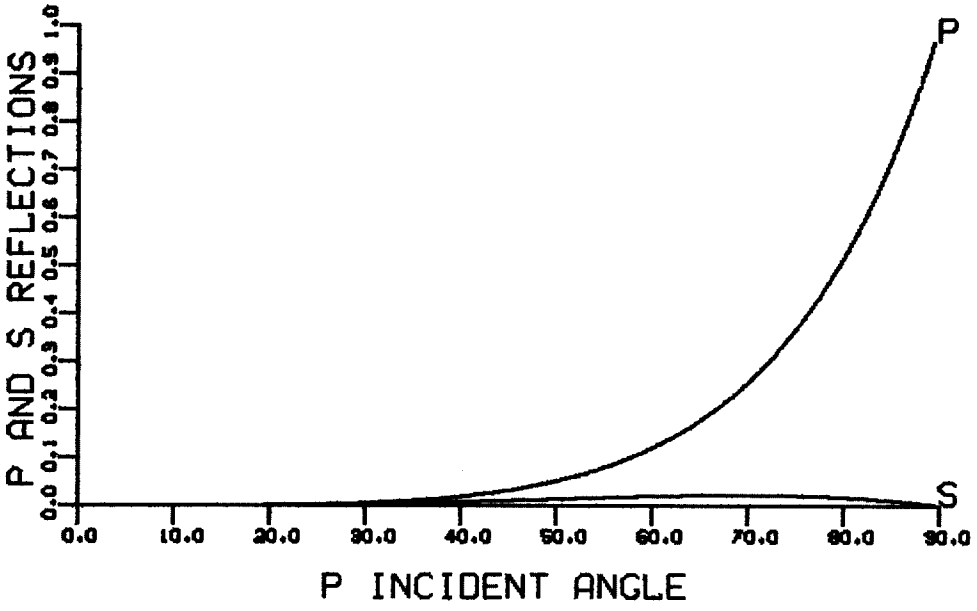
P AND S REFLECTIONS
0.0 0.1 0.2 0.3 0.4 0.5 0.6 0.7 0.8 0.9 1.0
P
S
0.0 10.0 20.0 30.0 40.0 50.0 60.0 70.0 80.0 90.0
P INCIDENT ANGLE

Figure 6.

The first example, Fig. 7, is a circularly spreading scalar wave. The Neumann conditions make the boundary act as a perfect reflector, but the absorbing boundary conditions allow the wave to pass through the grid perimeter.

The second example, Fig. 8, is a circular compressional elastic wave. Both the horizontal and vertical wave fields are depicted with "black" representing positive amplitudes and "white" representing negative amplitudes. A velocity ratio of $\alpha/\beta = \sqrt{3}$ was used.

The final example, Fig. 9, is a circular shear wave, and again $\alpha/\beta = \sqrt{3}$ was used.

Conclusions

A set of boundary conditions for scalar and elastic waves which minimize artificial reflections has been presented. The boundary conditions are essentially paraxial approximations of the scalar and elastic wave equations. The advantages of these boundary conditions are, first, that they absorb energy over a wide range of incident angles, and, second, that they are computationally inexpensive and simple to apply.

References

CLAERBOUT, J. F. [1970], "Course grid calculations of waves in inhomogeneous media with application to delineation of complicated seismid structure," *Geophysics* 35, pp. 407-418.

CLAERBOUT, J. F., and A. G. JOHNSON [1971], "Extrapolation of time dependent waveforms along their path of propagation," *Geophys. J. Roy. Astron. Soc.*, 26, pp. 285-295.

CLAERBOUT, J. F. [1976], *Fundamentals of Geophysical Data Processing* (New York: McGraw-Hill), pp. 163-226.

ENGQUIST, B. and A. MAJDA [1977], "Absorbing boundary conditions for the numerical simulation of waves,"

KELLY, K. R., R. W. WARD, S. TREITEL and R. M. ALFORD [1976], "Synthetic seismograms: A finite-difference approach," *Geophysics*, 41, pp. 2-27.

LYSMER, J. and R. L. KUHLEMEYER [1969], "Finite dynamic model for infinite media," *J. Eng. Mech. Div. ASCE*, 95 EM4, pp. 859-877.

SMITH, W. D. [1974], "A non-reflecting plane boundary for wave propagation problems," *J. Comp. Phys.*, 15, pp. 492-503.

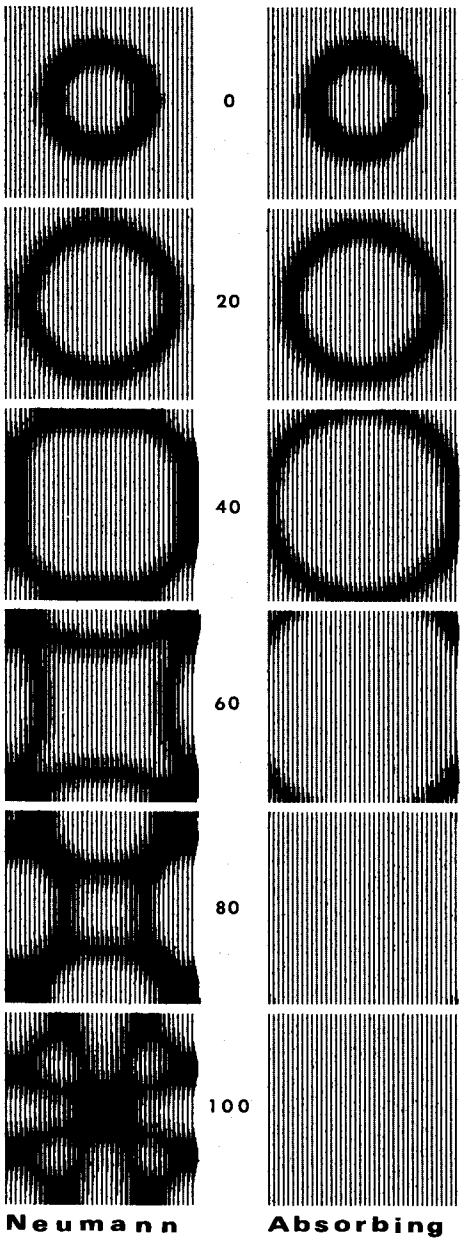

Figure 7.

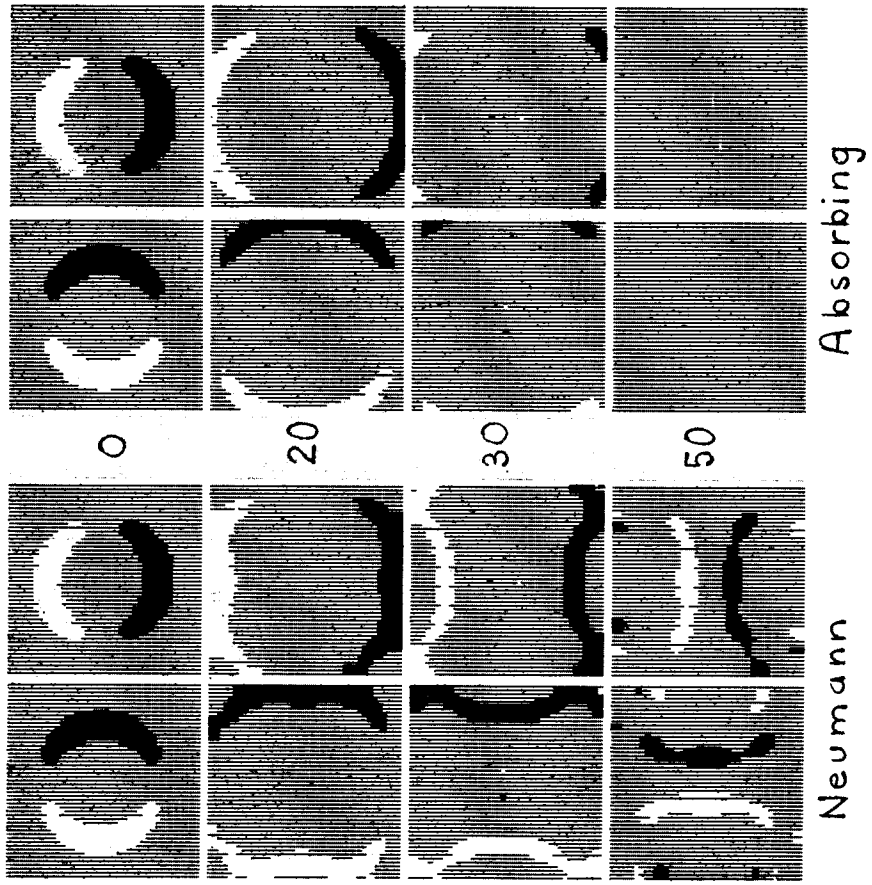

Figure 9.

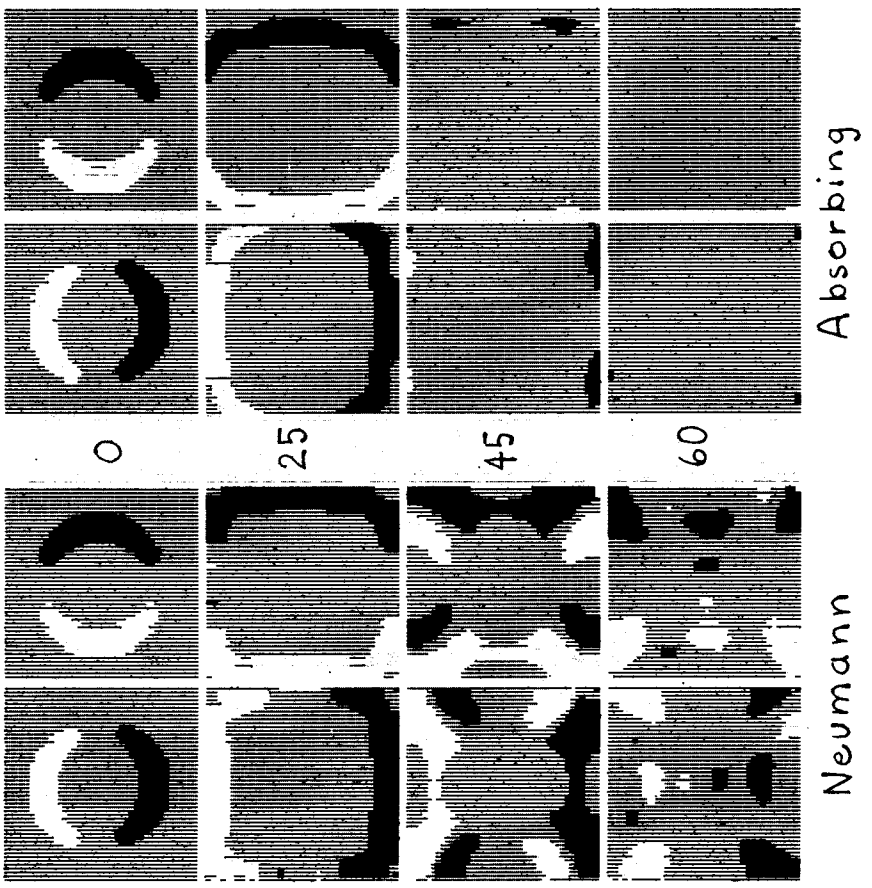

Figure 8.

APPENDIX

Finite Difference Schemes for Boundary Conditions

The finite difference formula for the second-order scalar paraxial approximation [Eq. (9)] is

$$D_+^z D_0^t P_{j,0}^n + \frac{1}{2v} D_+^t D_-^t (P_{j,0}^n + P_{j,1}^n) - \frac{v}{4} D_+^x D_-^x (P_{j+1,1}^n + P_{j-1,0}^n) = 0 ,$$

where

$$P_{j,k}^n = P(z_j, t_k, x^n) ,$$

and D_+^q, D_-^q, and D_0^q are respectively the forward, backward, and center difference operators with respect to the variable q.

For the second-order elastic boundary condition [Eq. (14)], the difference scheme is

$$D_+^z D_0^t \underline{u}_{j,0}^n + \frac{1}{2} C_1 D_+^t D_-^t (\underline{u}_{j,0}^n + \underline{u}_{j,1}^n) + \frac{1}{2} C_2 D_+^t D_0^x (\underline{u}_{j-1,0}^n + \underline{u}_{j,1}^n)$$

$$+ \frac{1}{2} C_3 D_+^x D_-^x (\underline{u}_{j-1,0}^n + \underline{u}_{j+1,1}^n) = 0 ,$$

where

$$\underline{u}(z_j, t_k, x^n) = \underline{u}_{j,k}^n .$$